SH 4.3.06

Basic Properties of Anomalous Cosmic Ray Spectra

H. Moraal and C.D. Steenberg*

Space Research Unit, Potchefstroom University for CHE, Potchefstroom 2520, South Africa
**Presently at SRU, California Institute of Technology, Pasadena, California 91125, USA*

Abstract

The anomalous cosmic ray component is a much more sensitive probe of modulation/acceleration in the heliosphere than galactic cosmic rays. Based on one-dimensional, no-drift solutions of the transport equation, we formulate several properties that govern their acceleration and modulation.

Introduction

In this paper we solve the cosmic ray transport equation

$$\frac{\partial f}{\partial t} = \nabla \cdot (\mathbf{K} \cdot \nabla f - f\ \mathbf{V}) + 1/3 (\nabla \cdot \mathbf{V}) \partial / \partial p (p^3 f) + Q \qquad (1)$$

numerically in a spherically symmetric heliosphere. This simple geometry is chosen to demonstrate a number of fundamental properties of anomalous cosmic ray (ACR) spectra that are useful to keep in mind when working with the solutions in more complicated geometries. The outer boundary is set at r_b = 120 AU, where the intensity is assumed zero. The solar wind termination shock (SWTS) is at r_s = 90 AU. This shock contains a source, $Q = Q_0 \delta(P\text{-}P_i)\delta(r\text{-}r_s)$, of particles, with an arbitrary magnitude Q_0, injected at P_i = 0.06 GV (1.9 MeV protons). The flux across the shock is discontinuous by an amount equal to this source strength. The radial diffusion mean free path inside the shock is $\lambda_{rr} = 0.5(P/P_0)^{\gamma}$ AU, independent of radial distance, where P_0 = 1GV. Outside the shock λ_{rr}, as well as the radial solar wind velocity of V = 400 km/s, are reduced by a factor s, which is the compression ratio of the shock. The radial grid contains 100 intervals inside, and 40 outside the shock. The rigidity grid has 2000 logarithmic intervals between 0.05 and 4 GV. The solution is started at t = 0 with an empty heliosphere, and updated every 0.11 days, until a quasi-steady state is reached after 16000 steps, for a total time of 4.85 years.

This simple solution is used to demonstrate the following properties and scalings. Evidently, each of them will change quantitatively in more comprehensive solutions.

1. The cutoff of the shock acceleration occurs at lower energies than is generally perceived. The full lines in Figure 1 show a solution of (1) for protons for γ =1. (The dashed line solutions will be discussed in Section 6). Figure 1b shows the spectrum that is accelerated on the SWTS for a strong shock, when s = 4, while Figure 1(a) shows the resulting modulated ACR spectra at radial distances r = 80, 60, 40, 20, and 1 AU, multiplied by $10^{0.5}$, 10^{0}, $10^{-0.5}$, 10^{-1}, and $10^{-1.5}$, respectively. In the standard first order Fermi mechanism, a plane, steady shock produces a kinetic energy spectrum of the form $j_T \propto P^2 f$, with $f \propto P^{-q}$, and $q = 3s/(s\text{-}1)$. Thus, for s =4, q =4, and in the non-relativistic case, $j_T \propto T^{-1}$. The straight, dashed line in Figure 1b with a slope of –1 demonstrates that the numerical solution of (1) produces the expected power law form.

This power law spectrum cuts off and rolls over into an exponential form at kinetic energy T_c = 37 MeV. This cutoff is due to the finite curvature of the shock and not due to the limited time available for the acceleration, because the solution was run long enough that it is in quasi-steady equilibrium. Many authors, *e.g.* Krymski *et al.* (1979) and Drury (1983), have discussed this curvature cutoff. The order of magnitude estimate is that it should occur when the diffusive length scale, κ_{rr}/V, becomes of the order shock radius, r_s, *i.e.* where $Vr_s/\kappa_{rr} \sim 1$. Our solution indicates however that it occurs much nearer to Vr_s/κ_{rr} = 10. It is easily shown that, when $\lambda_{rr} = \lambda_{rr0}(P/P_0)^{\gamma}$, the point where Vr_s/κ_{rr} = 10 occurs at a kinetic energy per nucleon, T_c, such that

$$(A/Z)^{\gamma} [(T_c (T_c + 2E_0)]^{(\gamma+1)/2} / (T_c + E_0) = 3Vr_s P_0^{\gamma} / (10c\lambda_{rr0}), \qquad (2)$$

where A and Z are the mass and charge numbers of the species. This cutoff energy is drawn in Figure 3 for Hydrogen and for singly charged Helium and Oxygen. When $\gamma = 1$, these cutoffs scale approximately $\propto (Z/A)$. This (Z/A) scaling is exact in *both* the relativistic and non-relativistic limits, but not in between.

The condition $Vr_s/\kappa_{rr} = 10$ and the cutoff energy in (2) are independent of shock strength. Figure 2b shows the same solution as in Figure 1b, except that the compression ratio is now $s = 2.5$. Using the same calculations as above, the power law index now is – 1.5, but the cutoff clearly occurs at the same energy, and the spectrum above the cutoff is of the same form as for the case $s = 4$ in Figure 1b.

2. ACR spectra are insensitive to the strength of the SWTS. They are predominantly determined by the shape of the SWTS spectrum above the cutoff. Figures 1a and 2a contain the modulated intensities produced by the SWTS spectra in Figures 1b and 2b. The shape and the peak energies of these two sets of solutions are quite similar. (The 1 AU intensity in Figure 2a just touches on the horizontal scale.) The biggest difference between these two sets is that the radial gradient (at the peak intensity) increases from ~ 8.0%/AU for the strong ($s = 4$) shock in Figure 1a, to ~ 9.6%/AU for the weak ($s = 2.5$) shock in Figure 2a.

This happens because the power law is produced for low energy particles which do not escape substantially from the SWTS and perceive it as plain, while the ACR spectra are composed of particles that penetrate deep into the heliosphere and, therefore, must sense the curvature of the SWTS.

We also notice that the shape of the SWTS spectrum and, therefore, modulated ACR spectra, as predicted by the solution of (1), are insensitive to (a) the injection energy as long as this energy is $< T_c$, and (b) shock structure. Injection and shock structure effects must be studied with complementary methods such as those of Ellison *et al*. (1999).

3. ACR intensities peak at roughly the same energy as the cutoff of the SWTS spectrum. The vertical dotted line in Figure 1a is drawn at the cutoff energy, T_c, of the SWTS spectrum. It shows that the peak intensity of the modulated anomalous spectra occurs in the vicinity of the cutoff energy. These intensity maxima shift to higher energy with decreasing radial distance, which is a natural consequence of the increasing amount of modulation. From 20 AU to 1 AU, however, the intensity maximum shifts back to lower energies, due to adiabatic energy losses that become important in the inner heliosphere. We know of no realistic way to produce ACR spectra with intensity maxima at substantially lower energy than the cutoff of the SWTS spectrum. Thus, we regard ACR intensity maxima as reliable markers of the cutoff energy.

4. The peak energy of ACR spectra is sensitive to the radial diffusion mean free path but not to drift effects. It follows from (2) that for the non-relativistic case the cutoff energy, T_c, is proportional to the strength of the modulation $(Vr_s/\lambda_{rr0})^{2/(\gamma+1)}$. Consequently, the entire SWTS spectrum, together with the modulated ACR spectra, shift in energy in proportion to this quantity. When $\gamma = 1$ ($\lambda_{rr} \propto P$) this means, for example, that if λ_{rr} is decreased by a factor a, all the spectra in Figures 1 and 2 shift a factor a towards higher energy. Simultaneously, because the power law sections of the spectra have a slope $2(s-1)/(s+2)$, all the intensities drop with a factor $2(s-1)/(s+2)/a$. For a strong shock, this factor is simply $1/a$. This scaling was confirmed with numerical solutions by Steenberg (1998). More generally, this scaling implies that the position in energy of anomalous spectra is proportional to $\int Vdr/\kappa_{rr}$. As modulation increases, the spectra shift to higher energies, and the intensities drop for two reasons: (i) there is the normal increased modulation as for galactic cosmic rays, and (ii) the upward shift of the cutoff, with the appropriate slope, reduces the intensity of the SWTS spectrum. These properties are widely known, but we are not aware that this simple scaling has been pointed out before.

Figures 5 and 6 are in the same format as Figures 1 and 2, but they are for a two-dimensional (radial distance, polar angle) positive and negative drift solutions of (1), respectively. The details of the solutions are given in

Steenberg (1998). The important points we stress here are that (i) SWTS spectra are greatly affected by these drifts, but (ii) the peak positions of ACR spectra are very similar to those of the no-drift one-1-D solutions of Figures 1 and 2, and there is no evidence that these peaks shift according to the sign of the drift .

5. The species scaling of ACR peaks provides an important diagnostic tool to study the modulation. If $\lambda_{rr} \propto P^{\gamma}$, or $\kappa_{rr} \propto \beta P^{\gamma}$, then, in a given heliosphere, species (1) and (2) have the same modulation if $(\beta P^{\gamma})_1 = (\beta P^{\gamma})_2$. This occurs at kinetic energies per nucleon such that

$$T_2 / T_1 = [(T_2 + 2E_0) / (T_2 + 2E_0)][(T_2 + E_0) / (T_1 + E_0)]^{2/(\gamma+1)}[(A_1 / Z_1) / (A_2 / Z_2)]^{2\gamma/(\gamma+1)} \quad (3)$$

This relationship is drawn in Figure 4 for H and He^{+}. The relativistic and non-relativistic limits are $T_2/T_1 = (A/Z)_1/(A/Z)_2$ and $T_2/T_1 = [(A/Z)_1/(A/Z)_2]^{2\gamma/(\gamma+1)}$, respectively. Thus, the β-dependence of κ_{rr} introduces a powerful diagnostic tool to study the rigidity dependence of the acceleration/modulation, but only for non-relativistic energies. Fortunately, all ACR spectra fall well into this non-relativistic range. When $\gamma = 1$ the non-relativistic scaling is also according to A/Z, and this is generally called total energy scaling because, if $Z = 1$, the positions of anomalous spectra scale according to total energy of the particles. Cummings and Stone (1998, and references therein) have done several studies along these lines since 1984. The present statement confirms the usefulness of these methods, and we point out that these studies are mainly useful for ACR's (rather than for GCR's) because they have, sharp, well-defined intensity maxima, which serve as useful "markers", and because their input spectra are produced by the same mechanism as the modulation.

6. A simple expression for the SWTS spectrum can be found in a spherically symmetric model. Steenberg (1998) and Steenberg and Moraal (1999) showed that the spectrum on the spherical SWTS can be modeled as $f \propto (P / P_c)^{-q} \exp[-b(P / P_c)^{2a}]$, which implies intensity spectra w.r.t. kinetic energy

$$j_T \propto (T / T_c)^{2-q} \exp[-b(T / T_c)^{2a}] \text{ and } j_T \propto (T / T_c)^{1-q/2} \exp[-b(T / T_c)^{a}] \quad (4)$$

in the relativistic and non-relativistic limits, respectively. The coefficients are given by $a = 0.689\gamma + 1.34$, and $b = -0.083\gamma + 0.272$, while T_c is given in terms of the species and modulation parameters by (2). The quality of fit is demonstrated by the dash-dot lines in Figures 1b and 2b. The dash-dot lines of Figures 1a and 2a are steady state solutions of (1), using these analytical expressions for the SWTS spectra as input. Clearly, these spectra fit the full solutions exceedingly well, and the method is highly useful because the steady state solution of (1) is at least 2000 times faster than the time-dependent solution.

References

Cummings, A.C. and E.C. Stone, 1998. *Space Sci. Rev.* **83**, 51

Drury, L.O'C. 1983. *Rep. Prog. Phys.,* **46,** 973.

Ellison, D.C., F.C. Jones, and M.G. Baring, 1999, *Astrophys. J.,* **512**, 403

Krymski, G.F., A.I. Kuzmin, and S.I. Petukhov. 1979. *Proc. 16th Int. Cosmic Ray Conf. (Kyoto),* **2**, 44

Steenberg, C.D. 1998. Ph.D. thesis, Potchefstroom University, Potchefstroom, South Africa

Steenberg, C.D. and H. Moraal, 1999. The form of the anomalous cosmic ray spectrum at the solar wind termination shock. Submitted to *J. Geophys. Res.*

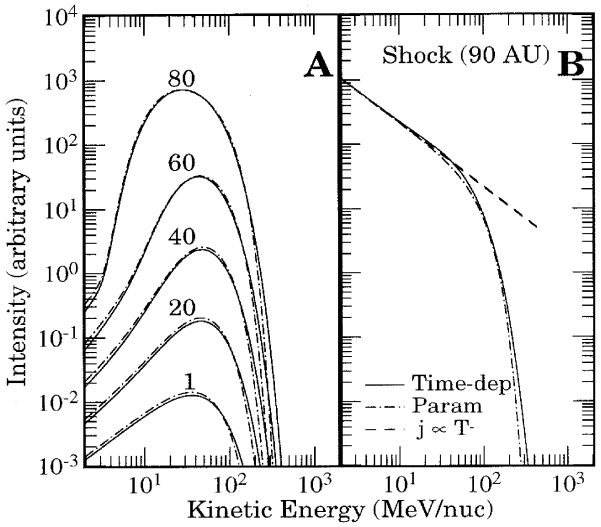

Figure 1

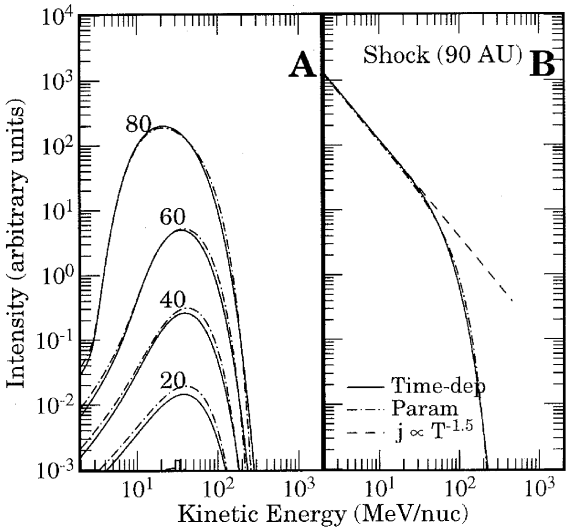

Figure 2

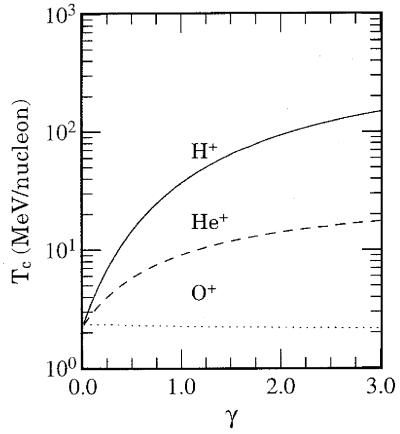

Figure 3

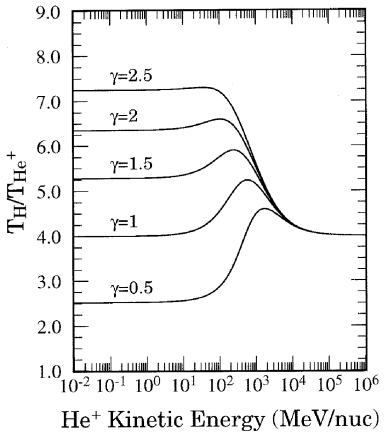

Figure 4

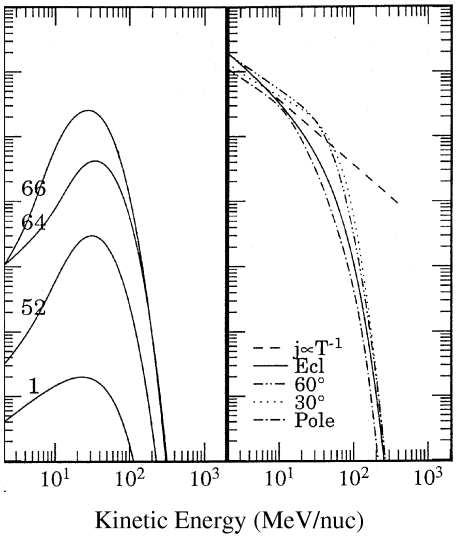

Figure 5

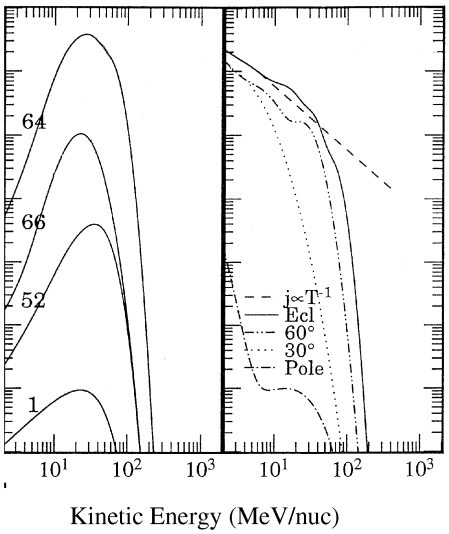

Figure 6